Zhao *et al. Intell Robot* 2024;4(4):339-62
DOI: 10.20517/ir.2024.21

Intelligence & Robotics

Research Article

Open Access

Check for updates

Neurodynamics-based formation tracking control of leader-follower nonholonomic multiagent systems

Xiao-Wen Zhao[1], Meng-Ke Li[1], Qiang Lai[2], Zhi-Wei Liu[3]

[1]School of Mathematics, Hefei University of Technology, Hefei 230601, Anhui, China.
[2]School of Electrical and Automation Engineering, East China Jiaotong University, Nanchang 330013, Jiangxi, China.
[3]School of Automation, Huazhong University of Science and Technology, Wuhan 430074, Hubei, China.

Correspondence to: Prof. Xiao-Wen Zhao, School of Mathematics, Hefei University of Technology, 420 Feicui Road, Shushan District, Hefei 230601, Anhui, China. E-mail: zhaoxiaowen@hfut.edu.cn

How to cite this article: Zhao XW, Li MK, Lai Q, Liu ZW. Neurodynamics-based formation tracking control of leader-follower nonholonomic multiagent systems. *Intell Robot* 2024;4(4):339-62. http://dx.doi.org/10.20517/ir.2024.21

Received: 25 Jul 2024 **First Decision:** 23 Sep 2024 **Revised:** 21 Oct 2024 **Accepted:** 1 Nov 2024 **Published:** 13 Nov 2024

Academic Editors: Simon Yang, Jianjun Ni **Copy Editor:** Pei-Yun Wang **Production Editor:** Pei-Yun Wang

Abstract

This paper uses a bioinspired neurodynamic (BIN) approach to investigate the formation control problem of leader-follower nonholonomic multiagent systems. In scenarios where not all followers can receive the leader's state, a distributed adaptive estimator is presented to estimate the leader's state. The distributed formation controller, designed using the backstepping technique, utilizes the estimated leader states and neighboring formation tracking error. To address the issue of impractical velocity jumps, a BIN-based approach is integrated into the backstepping controller. Furthermore, considering the practical applications of nonholonomic multiagent systems, a backstepping controller with a saturation velocity constraint is proposed. Rigorous proofs are provided. Finally, the effectiveness of the presented formation control law is illustrated through numerical simulations.

Keywords: Leader-follower formation control, distributed estimation, nonholonomic multiagent systems, bioinspired neurodynamics, constrained control

1. INTRODUCTION

In recent years, the distributed cooperative control of multiagent systems has received extensive attention from the control engineering research community due to its potential in various practical applications[1–3]. Examples of cooperative of multiagent systems include consensus[4], flocking[5], synchronization[6], rendezvous[7],

and formation[8]. Formation control, as an active research topic in this field, finds extensive applications in traffic control, logistics transportation, distributed prediction, monitoring, and diagnosis[9–14]. The main goal of multiagent formation control is to coordinate and control multiple agents to reach and maintain a specific formation by designing a controller.

Most of the existing research papers on formation control are applied to solve the kinematic modeling of a single integrator or double integrator. However, the multiagent systems with nonholonomic constraints in formation control are a more realistic model. Due to the characteristics of the nonholonomic motion model, the agent cannot freely rotate or slide, which makes our design more challenging. Among the various formation control laws and methods, the leader-follower method has gained popularity due to its simplicity and ease of control. In[15], the study focuses on the leader-follower flexible formation controller without considering the global pose measurement information for a class of nonholonomic mobile robots. Considering the various constraints existing in practical applications[16], studied the problem of formation constraints, such as feasibility, communication, and performance constraints for nonholonomic systems in the leader-follower framework. In[17], an embedded control technique is proposed to split the formation controller task into two parts, which improves the generality and scalability of the controller. However, common to all the aforementioned literature is the context in which all followers have knowledge of the state information of the leader. Considering the packet loss in communication and the limited bandwidth, it seems more reasonable to assume that just a portion of neighboring robots can receive the leader's state. To address this issue[18], proposed a linear protocol to estimate the position and orientation of the Leader and used a sliding mode approach to estimate the linear velocity of the leader. However, designed an adaptive edge-event-triggered observer to estimate the matrix and state of the leader[19]. In[18], it is assumed that the upper bound of the linear velocity of the Leader is known, which is not easy in practical applications. Therefore, it is necessary to study a practical distributed estimator for estimating the state information of the leader.

The literature lists various tracking control methods for multiagent systems, including neural network and fuzzy system control[20,21], robust control[22], iterative learning control[23], sliding mode control[24], and backstepping control[25–27]. Among these methods, the backstepping approach is often preferred. The utilization of the backstepping technique not only simplifies the tracking controller but also ensures system stability by leveraging the Lyapunov stability theory. For instance,[25] proposed a hybrid backstepping control strategy based on neural networks for nonholonomic systems with unknown wheel slips and external disturbances. Similarly, in[26], the study presented a backstepping control strategy based on the saturation adaptive law for uncertain nonlinear systems with external dynamic disturbances. However, traditional backstepping-based controllers may experience unrealistic velocity jumps when encountering sudden changes in tracking errors, causing the robot to start at a very high-velocity value. To address this, a bioinspired neurodynamic (BIN) approach developed from the Hodgkin and Huxley membrane equations was introduced in[28]. In[29], the authors developed a BIN-based tracking controller for the nonholonomic mobile robot that generates steady and continuous control signals. Similarly, presents a novel BIN approach to the formation control of underactuated systems under uncertain dynamics[30]. Recent research by ref[31] has investigated trajectory tracking control for wheeled mobile robots using the BIN technique. Inspired by the problem of designing control in biological models, this paper combines backstepping techniques with a neurodynamic model to design a nonholonomic multiagent controller to solve the velocity jump problem.

In practice scenarios, the motors of nonholonomic multiagents are constrained by technical limitations, resulting in a saturation constraint on the velocity of the nonholonomic system. Large tracking errors can cause the control input to exceed the system's allowed speed range, leading to the nonholonomic multiagent sliding and violating the nonholonomic constraint. In fact, a lot of ground vehicles and most aircraft are subject to this physical constraint. Examples include fixed-wing drones and flying robots[32–34]. Therefore, investigating the formation control issue of a group of nonholonomic multiagents under velocity limitations is crucial. Moti-

vated by the above observations, this paper presents a distributed formation control approach that utilizes the backstepping technique with BIN modeling for the formation control of leader-follower nonholonomic multi-agents. The technical difficulties mainly stem from that: (1) A distributed estimator is designed to estimate the leader's velocity under the assumption that the desired velocity boundary is unknown; (2) Unrealistic velocity jumps occur when using backstepping controllers to implement formation control problem; (3) The formation controller with velocity constraints is further investigated. The main contribution can be summarized as follows:

1. A distributed observer is proposed to estimate the leader's state. Unlike the approaches in references[34] and[35] that assume the desired velocity has known boundaries during implementation and design, we propose an adaptive estimator with dynamic control gain. This eliminates the need for assuming known velocity bounds and enables the estimation of the leader's linear velocities and leader's angular velocities. By incorporating this observer, the followers can estimate the velocity of the leader, which is essential for formation control.
2. The proposed control strategy employs a bioinspired backstepping controller for a group of nonholonomic mobile robots. This controller addresses the issue of impractical velocity jumps commonly encountered in traditional backstepping-based controllers. By leveraging the BIN approach, which is derived from biological nervous systems, the control signals generated by the controller are continuous and smooth. This ensures that the robots' velocities do not experience abrupt changes, leading to better tracking performance and improved stability. Additionally, the introduction of tracking errors of neighborhood formation enhances the effectiveness of the algorithm, enabling tighter formation control.
3. In practical scenarios, nonholonomic mobile robots often have velocity constraints due to motor limitations. To account for this, a saturated velocity constrained controller is designed in the proposed strategy. This controller prevents input saturation caused by velocity saturation, ensuring that the control inputs remain within the allowable velocity range of the robots. By considering the velocity constraints, the control strategy ensures that the nonholonomic constraints are respected, preventing the robots from sliding and maintaining their intended motion. In addition, compared with literature[34], our designed controller can achieve the formation objective with a faster convergence rate while satisfying the same constraints.

The outline of this paper is presented as follows. In Section 2, the mathematical foundations and the formulation of the problem are presented. Section 3 proposes the distributed estimator and error dynamics. Section 4 covers the BIN model and the design of formation control strategy. In Section 5, the case of saturated velocity constraints is considered. Finally, Section 6 presents numerical simulation results to demonstrate the effectiveness of the controller.

2. PRELIMINARIES AND PROBLEM STATEMENT

2.1 Algebraic graph theory

Let $\mathcal{G} = (\mathcal{V}, \mathcal{E})$ denote undirected graph interactions among agents, where $\mathcal{V} = \{1, \ldots, N\}$ is the node set and $\mathcal{E} \subseteq \mathcal{V} \times \mathcal{V}$ is the edge set. The edge between the node $i, j \in \mathcal{V}$ is bidirectional. An edge $(j, i) \in \mathcal{E}$ denotes that the information of node i can be obtained by the node j. Let $\mathcal{A} = [a_{ij}]_{n\times n}$ be the adjacency matrix as defined as follows: $a_{ij} > 0$ if $(j, i) \in \mathcal{E}$; otherwise, $a_{ij} = 0$. In this work, we assume that $a_{ii} = 0$ for all agents i. The set of neighbors of agents i is denoted by $\mathcal{N}_i := \{j \in \mathcal{V} | (i, j) \in \mathcal{E}\}$. The Laplacian matrix $\mathcal{L} = [l_{ij}]$ is defined as $l_{ij} = -a_{ij}$ if $j \neq i$, and $l_{ij} = \sum_{j=1}^{N} a_{ij}$ if $j = i$.

In this paper, the followers are represented by nodes $\{1, \ldots, N\}$, and the leader is represented by the node r. $\bar{\mathcal{G}}$ is an undirected augmented graph with $\bar{\mathcal{V}} = \mathcal{V} \cup \{r\}$. The interaction between each follower and leader can be expressed as a diagonal matrix $\mathcal{B} = diag(b_1, \ldots, b_N)$ with $b_i = 1$ if the leader is a neighbor of follower i, and otherwise $b_i = 0$. Finally, define matrix $\mathcal{H}$ as

$$H = \mathcal{L} + \mathcal{B}. \tag{1}$$

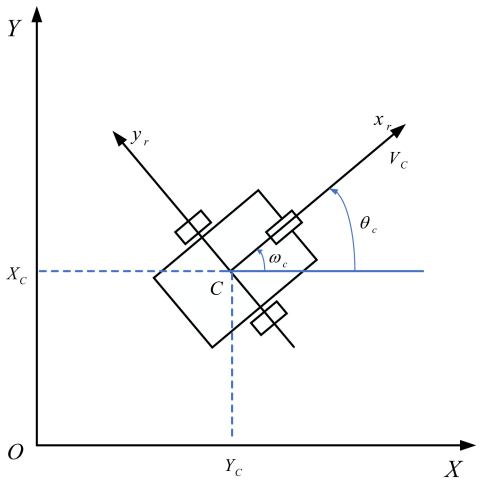

Figure 1. Configuration of the nonholonomic mobile robot.

2.2 Problem Formulation

A multi-robot system with $N+1$ nonholonomic multiagents, where N followers and one leader are considered. A typical configuration of them is shown in Figure 1. For each follower, the kinematics can be expressed as

$$\begin{cases} \dot{x}_i = v_i \cos\theta_i, \\ \dot{y}_i = v_i \sin\theta_i, \\ \dot{\theta}_i = \omega_i, \end{cases} \tag{2}$$

where $p_i = [x_i, y_i]^{\mathrm{T}} \in \mathbb{R}^2$ and θ_i are the position of the center of mass and the orientation of each agent i, respectively. $v_i \in \mathbb{R}$ and $\omega_i \in \mathbb{R}$ are the linear velocity and angular velocity of agents i, respectively, which also are the control input. The leader's kinematics is given as

$$\begin{cases} \dot{x}_r = v_r \cos\theta_r, \\ \dot{y}_r = v_r \sin\theta_r, \\ \dot{\theta}_r = \omega_r, \end{cases} \tag{3}$$

where $p_r = [x_r, y_r]^{\mathrm{T}} \in \mathbb{R}^2$ is the position coordinates and θ_r is the orientation, respectively. $v_r \in \mathbb{R}$ is the linear velocity and $\omega_r \in \mathbb{R}$ is the angular velocity.

The objective of the formation control is to develop a formation control law that ensures each follower maintains a specific position and orientation in relation to the leader. In this work, the desired relative position of the agent i with respect to the reference position p_r is defined as $\Delta_i = [\Delta_{ix}, \Delta_{iy}]^{\mathrm{T}} \in \mathbb{R}^2$, and we expect all follower agents to have the same orientation as the leader agent.

The formation control problem in this paper is then stated as follows.

Problem 1 Consider $N+1$ nonholonomic multiagents and the network topology $\bar{\mathcal{G}}$. For each follower i in (2), develop the control law (v_i, ω_i) to align the orientation with the leader and hold the desired geometrical shape, as follows:

$$\lim_{t\to\infty} (p_r(t) - p_i(t) + \Delta_i) = 0, \tag{4}$$

$$\lim_{t\to\infty} (\theta_r(t) - \theta_i(t)) = 0. \tag{5}$$

The following lemma and assumptions are used to address the proposed formation control problem.

Assumption 1 The undirected augmented graph $\bar{\mathcal{G}}$ has a spanning tree in which the root of the spanning tree is the leader.

Remark 1 Given the aforementioned assumption, matrix H is symmetric positive definite.

Assumption 2 The desired velocity v_r, ω_r and acceleration $\dot{v}_r, \dot{\omega}_r$ are both bounded.

Considering that only a portion of robots can receive the leader's state, an estimator will be developed to estimate the leader's states. To facilitate the estimator design analysis, we provide the technical lemma as follows.

Lemma 1 (Nonsmooth Barbalat's Lemma [36]) Assume that for all $t \geq t_0$, there exists a compact set Ω such that the Filippov solution of $\dot{x} = f(x,t)$ always remains within it. If $\dot{\tilde{U}}$ is an empty set, there is a regular function of the change over time $U : \Omega \to \mathbb{R}$ with $v \leq 0\ \forall v \in \dot{\tilde{U}}$ is ordinary. So in Ω, all trajectories will converge to a fixed point s, where s belongs to $S = \{x \in \Omega | 0 \in \dot{\tilde{U}}\}$ closure.

3. ESTIMATION AND CONTROL DESIGN

This section first establishes the distributed estimator. Next, the error dynamics system is built, and the backstepping controller is presented to control the nonholonomic multiagents.

3.1 The proposed distributed estimator

The following distributed estimators of estimating the leader's states are defined as

$$\begin{cases} \dot{x}_{ir} = v_{ir}\cos\theta_{ir} + \sum_{j=N_i}^{n} a_{ij}\left(x_{jr} - x_{ir}\right) + b_i\left(\hat{x}_r - x_{ir}\right), & (6a) \\ \dot{y}_{ir} = v_{ir}\sin\theta_{ir} + \sum_{j=N_i}^{n} a_{ij}\left(y_{jr} - y_{ir}\right) + b_i\left(\hat{y}_r - y_{ir}\right), & (6b) \\ \dot{\theta}_{ir} = \omega_{ir} + \sum_{j=N_i}^{n} a_{ij}\left(\theta_{jr} - \theta_{ir}\right) + b_i\left(\hat{\theta}_r - \theta_{ir}\right), & (6c) \\ \dot{v}_{ir} = \left(\sum_{j=N_i}^{n} a_{ij}\left(v_{jr} - v_{ir}\right) + b_i\left(v_r - v_{ir}\right)\right) + \sum_{j=N_i}^{n} c_{ij}a_{ij}sign\left(v_{jr} - v_{ir}\right) + c_i b_i sign\left(\hat{v}_r - v_{ir}\right), & (6d) \\ \dot{\omega}_{ir} = \left(\sum_{j=N_i}^{n} a_{ij}\left(\omega_{jr} - \omega_{ir}\right) + b_i\left(\omega_r - \omega_{ir}\right)\right) + \sum_{j=N_i}^{n} d_{ij}a_{ij}sign\left(\omega_{jr} - \omega_{ir}\right) + d_i b_i sign\left(\hat{\omega}_r - \omega_{ir}\right). & (6e) \end{cases}$$

The adaptive weights c_{ij}, c_i, d_{ij}, d_i are updated by

$$\dot{c}_{ij} = \sigma_1\left\|v_{jr} - v_{ir}\right\|_1,\ \dot{c}_i = \sigma_1\|\hat{v}_r - v_{ir}\|_1, \quad (7)$$

$$\dot{d}_{ij} = \sigma_2\left\|\omega_{jr} - \omega_{ir}\right\|_1,\ \dot{d}_i = \sigma_2\|\hat{\omega}_r - \omega_{ir}\|_1, \quad (8)$$

where $x_{ir}, y_{ir}, \theta_{ir}, v_{ir}, \omega_{ir}$ are estimates of $x_r, y_r, \theta_r, v_r, \omega_r$ obtained by each robot i, and $\hat{x}_r \equiv x_r, \hat{y}_r \equiv y_r, \hat{\theta}_r \equiv \theta_r, \hat{v}_r \equiv v_r, \hat{\omega}_r \equiv \omega_r$. Additionally, σ_1, σ_2 are positive control gains.

Theorem 1 Consider nonholonomic multiagent systems (2). Assuming that Assumption 1 holds, by choosing suitable control gains σ_1 and σ_2, the distributed estimator (6) is capable of asymptotically estimating the state of the leader agent, including x_r, y_r, θ_r, v_r, and w_r.

Proof. Define the estimate error of each agent as $\tilde{x} := \hat{x} - x_r 1_N$, $\tilde{y} := \hat{y} - y_r 1_N$, $\tilde{\theta} := \hat{\theta} - \theta_r 1_N$, $\tilde{v} := \hat{v}_r 1_N$, $\tilde{\omega} := \hat{\omega}_r 1_N$, where $\hat{x} = (x_{1r}, \ldots, x_{Nr})^{\mathrm{T}}$, $\hat{y} = (y_{1r}, \ldots, y_{Nr})^{\mathrm{T}}$, $\hat{\theta} = (\theta_{1r}, \ldots, \theta_{Nr})^{\mathrm{T}}$, $\hat{v} = (v_{1r}, \ldots, v_{Nr})^{\mathrm{T}}$, $\hat{\omega} = (\omega_{1r}, \ldots, \omega_{Nr})^{\mathrm{T}}$.

Then, rewrite (6) in the matrix-vector form, as given below

$$\begin{cases} \dot{\hat{x}} = diag(\cos\hat{\theta})\hat{v} - H\tilde{x}, & (9a)\\ \dot{\hat{y}} = diag(\sin\hat{\theta})\hat{v} - H\tilde{y}, & (9b)\\ \dot{\hat{\theta}} = \hat{\omega} - H\tilde{\theta}, & (9c)\\ \dot{\tilde{v}} \in -H\tilde{v} + \mathcal{F}\left[-LC_1 sign\left(L\tilde{v}\right) - BC_2 sign(\tilde{v}) - (1_N \otimes \dot{v}_r)\right], & (9d)\\ \dot{\tilde{\omega}} \in -H\tilde{\omega} + \mathcal{F}\left[-LD_1 sign(L\tilde{\omega}) - BD_2 sign(\tilde{\omega}) - (1_N \otimes \dot{\omega}_r)\right]. & (9e) \end{cases}$$

Since the sign functions in (6d) and (6e) are discontinuous, a nonsmooth analysis will be performed to investigate their stability. For this purpose, the Filippov solution of (6d) and (6e) is defined as to be an absolutely continuous differential inclusion solution, as (9d) and (9e), respectively. $C_1 \equiv diag(c_{ij})$, $C_2 \equiv diag(c_i)$, $D_1 \equiv diag(d_{ij})$, $D_2 \equiv diag(d_i)$.

Choose the Lyapunov function candidate for (9d)

$$V_1 = \frac{1}{2}\tilde{v}^T\tilde{v} + \frac{1}{2}\sum_{i=1}^{N}\sum_{j\in N_i}\frac{(c_{ij} - c_e^*)^2}{\sigma_1} + \frac{1}{2}\sum_{i=1}^{l}\frac{(c_i - c_p^*)^2}{\sigma_1}, \tag{10}$$

where the positive constants c_e^* and c_p^* will be determined later. The set-valued Lie derivative of V_1 along the solution of (9d) is

$$\begin{aligned} \dot{V}_1 =& \tilde{v}^T\dot{\tilde{v}} + \sum_{i=1}^{N}\sum_{j\in N_i}\frac{(c_{ij} - c_e^*)}{\sigma_1}\dot{c}_{ij} + \sum_{i=1}^{l}\frac{(c_i - c_p^*)}{\sigma_1}\dot{c}_i \\ =& -\tilde{v}^T H\tilde{v} + \mathcal{F}\Bigg[-\tilde{v}^T Lc_1 sign\left(L\tilde{v}\right)\tilde{v}^T c_2 B sign(\tilde{v}) - \tilde{v}^T\left(1_N \otimes \dot{v}_r\right) \\ &+ \sum_{i=1}^{N}\sum_{j\in N_i}(c_{ij} - c_e^*)\left\|\tilde{v}_j - \tilde{v}_i\right\|_1 + \sum_{i=1}^{l}(c_i - c_p^*)\|\tilde{v}\|_1\Bigg]. \end{aligned} \tag{11}$$

Notice that by using $\delta sign(\delta) = \|\delta\|_1$ [32], we can get

$$\tilde{v}^T Lc_1 sign\left(L\tilde{v}\right) = \sum_{i=1}^{N}\sum_{j\in N_i} c_{ij}\left\|\tilde{v}_j - \tilde{v}_i\right\|_1, \tag{12}$$

$$\tilde{v}^T Bc_2 sign\left(\tilde{v}\right) = \sum_{i=1}^{l} c_i\|\tilde{v}\|_1. \tag{13}$$

In addition

$$\begin{aligned} \tilde{v}^T\left(1_N \otimes \dot{v}_r\right) &= \tilde{v}^T HH^{-1}\left(1_N \otimes \dot{v}_r\right) \\ &\le \|H\tilde{v}\|_1\left\|H^{-1}\left(1_N \otimes \dot{v}_r\right)\right\|_\infty \\ &\le \frac{\rho}{\lambda_{\min}(H)}\left(\sum_{i=1}^{N}\sum_{j\in N_i}\left\|\tilde{v}_j - \tilde{v}_i\right\|_1 + \sum_{i=1}^{l}\|\tilde{v}\|_1\right). \end{aligned} \tag{14}$$

Then, combining (11)-(14) yields, we can get

$$\dot{V}_1 \leq -\tilde{v}^T H\tilde{v} + \mathcal{F}\left[-\sum_{i=1}^{N}\sum_{j\in N_i}\left(c_e^* - \frac{\rho}{\lambda_{\min}(H)}\right)\left\|\tilde{v}_j - \tilde{v}_i\right\|_1 - \sum_{i=1}^{l}\left(c_p^* - \frac{\rho}{\lambda_{\min}(H)}\right)\|\tilde{v}\|_1\right]. \tag{15}$$

Choosing $c_e^* > \frac{\rho}{\lambda_{\min}(H)}$, $c_p^* > \frac{\rho}{\lambda_{\min}(H)}$, such that $\dot{V}_1 \leq -\tilde{v}^T H\tilde{v}$, H is positive definite matrix, so $\tilde{v}$ asymptotically converges to 0_N .

Likewise, consider Lyapunov function $V_2 = \frac{1}{2}\tilde{\omega}^T\tilde{\omega} + \frac{1}{2}\sum_{i=1}^{N}\sum_{j\in N_i}\frac{(d_{ij}-d_e^*)^2}{\sigma_2} + \frac{1}{2}\sum_{i=1}^{l}\frac{(d_i-d_p^*)^2}{\sigma_2}$. The set-valued Lie derivative of V_2 along the solutions of (9e) also can be derived, yielding $\dot{V}_2 \leq -\tilde{\omega}^T H\tilde{\omega} \leq 0$. So, $\tilde{\omega}$ converges to 0_N asymptotically.

Next, we consider the estimation dynamics (9c) for θ_{ir}. The estimation error's time derivative is provided by

$$\dot{\tilde{\theta}} = -H\tilde{\theta} + \hat{\omega} - \omega_r 1_N = -H\tilde{\theta} + \tilde{\omega}.$$

We can get the solutions as $\tilde{\theta} = e^{-Ht}\tilde{\theta}(0) + \int_0^t e^{-H(t-s)}\tilde{\omega}(s)ds$. Because the matrix H is Hurwitz and $\tilde{\omega}$ asymptotically converges to 0_N, we have

$$\lim_{t\to\infty}\tilde{\theta} = \lim_{t\to\infty}e^{-Ht}\tilde{\theta}(0) + \lim_{t\to\infty}\int_0^t e^{-H(t-s)}\tilde{\omega}(s)ds = 0_N.$$

Therefore, it can be said that $\tilde{\theta}$ converges to 0_N asymptotically.

In addition, we can obtain from (9a),

$$\dot{\tilde{x}} = diag\left(\cos\hat{\theta}\right)(\hat{v} - v_r 1_N) + v_r diag\left(\cos\hat{\theta} - \cos\theta_r 1_N\right) - H\tilde{x}.$$

Inspired by the above, let $\bar{\omega} := diag\left(\cos\hat{\theta}\right)(\hat{v} - v_r 1_N) + v_r diag\left(\cos\hat{\theta} - \cos\theta_r 1_N\right)$. Then, $\tilde{x} = e^{-Ht}\tilde{v}(0) + \int_0^t e^{-H(t-s)}\bar{\omega}(s)ds$. Since $\tilde{\theta}$ and $\tilde{v}$ asymptotically converge to 0_N, we have

$$\lim_{t\to\infty}\bar{\omega} = \lim_{t\to\infty}diag\left(\cos\hat{\theta}\right)(\hat{v} - v_r 1_N) + \lim_{t\to\infty}v_r diag\left(\cos\hat{\theta} - \cos\theta_r 1_N\right) = 0_N.$$

Consequently, it can be verified that $\tilde{x}$ converges to 0_N asymptotically. In the same way, it can be demonstrated that $\tilde{y}$ converges to 0_N asymptotically. This completes the proof.

Remark 1 In this paper, we assume that only part of the followers can obtain the state information x_r, y_r, θ_r, v_r, ω_r of the leader. This part is reflected as the neighbors of the leader in the paper, and b_i is used to represent the interaction relationship between the follower and the leader. If follower i is the neighbor of the leader, $b_i = 1$, otherwise $b_i = 0$. The variables x_r, y_r, θ_r, v_r, ω_r in estimator (6) are used on the premise that $b_i = 1$, meaning that the agent is a neighbor of the leader and can obtain the state x_r, y_r, θ_r, v_r, ω_r of the leader, satisfying our assumption. For clarity of presentation, we use $\hat{x}_r$, $\hat{y}_r$, $\hat{\theta}_r$, $\hat{v}_r$, $\hat{\omega}_r$ instead of x_r, y_r, θ_r, v_r, ω_r, where $\hat{x}_r \equiv x_r$, $\hat{y}_r \equiv y_r$, $\hat{\theta}_r \equiv \theta_r$, $\hat{v}_r \equiv v_r$, $\hat{\omega}_r \equiv \omega_r$. This notation makes the expression of the estimator more rigorous.

Remark 2 Noteworthy is the fact that equations (7) and (8) present an adaptive dynamic control law that depends entirely on the estimation errors. Therefore, it is not necessary to determine the desired velocity's bound. In equation (6), the sign function enables the asymptotically estimation of the leader's information. However, if you substitute a sigmoid or saturation function for the sign function, you can avoid chattering. The downside is that you will lose the ability to reconstruct the leader's state asymptotically.

3.2 Tracking error and error dynamics

This section discusses the scenario where certain follower agents are only aware of their intended relative position in relation to other follower agents. Using the leader's estimated states, the following defines the formation tracking errors

$$\tilde{p}_i = p_{ir} - p_i + \Delta_i, \quad \tilde{\theta}_i = \theta_{ir} - \theta_i, \tag{16}$$

Then, the tracking error system is given as

$$\dot{\tilde{p}}_i = R^T(\theta_i) \begin{bmatrix} v_{ir}\cos\tilde{\theta}_i - v_i \\ v_{ir}\sin\tilde{\theta}_i \end{bmatrix} + \varrho_i, \quad \dot{\tilde{\theta}}_i = \dot{\theta}_{ir} - \omega_i, \tag{17}$$

where $R(\theta_i)$ and ϱ_i are given by

$$R(\theta_i) = \begin{bmatrix} \cos\theta_i & \sin\theta_i \\ -\sin\theta_i & \cos\theta_i \end{bmatrix}, \varrho_i = \begin{bmatrix} \dot{x}_{ir} - v_{ir}\cos\theta_{ir} \\ \dot{y}_{ir} - v_{ir}\sin\theta_{ir} \end{bmatrix}.$$

The neighborhood formation tracking error is designed in the control law to prevent relying solely on the tracking error $\tilde{p}_i$. Define

$$e_i = \sum_{j=1}^{n} a_{ij}\left(p_j - p_i + \Delta_{ij}\right) + b_i\tilde{p}_i, \tag{18}$$

Below is the distributed formation controller based on a typical backstepping technique.

$$\begin{aligned} v_i &= v_{ir}\cos\tilde{\theta}_i + k_1\tilde{x}_i, \\ \omega_i &= k_2\tilde{\theta}_i + \dot{\theta}_{ir} + k_3\frac{\sin\tilde{\theta}_i}{\tilde{\theta}_i}v_{ir}\tilde{y}_i, \end{aligned} \tag{19}$$

where k_1, k_2, and k_3 are positive constants. However, the current formation controller, which is based on the backstepping technique, has an issue with velocity jumps. After analyzing it, we found that the velocity jumps occur due to abrupt changes in the tracking error, specifically $\tilde{\theta}_i$. To enhance the controller's efficiency and performance, we have introduced a BIN model into the backstepping control.

4. THE BIN CONTROLLER DESIGN

4.1 The bioinspried neurodynamics model

Using circuit elements, Hodgkin and Huxley developed a membrane block model of a biological neural system. In their membrane block model, the state equation of voltage across the membrane V_m is given as follows.

$$C_m\dot{V}_m = -(E_p + V_m)g_p + (E_{Na} - V_m)g_{Na} - (E_k + V_m)g_k \tag{20}$$

where C_m is the membrane capacitance, and E_k, E_{Na}, and E_p are the Nernst potentials for the potassium ions, the sodium ions, and the passive leak current, respectively. In addition, the parameters g_k, g_{Na} and g_p are the Conductance of potassium, Conductance of sodium and Conductance of passive channels, respectively. By setting $C_m = 1$ and substituting $x_i = E_p + V_m$, $A_i = g_p$, $B_i = E_{Na} + E_p$, $D_i = E_k - E_p$, $S_i^+ = g_{Na}$, and $S_i^- = g_k$. Later, a typical shunting neural dynamic model was derived as follows

$$\dot{x}_i = -A_i x_i + (B_i - x_i)S_i^+(t) - (D_i + x_i)S_i^-(t). \tag{21}$$

The i-th neuron's neuronal activity is represented by the equation, involving the membrane potential x_i, non-negative constants A_i, B_i, and D_i representing passive decay rate, upper bounds and lower bounds. Variables S_i^+ and S_i^- express excitatory and inhibitory inputs. The BIN model has the following properties: (1) For arbitrary excitatory and inhibitory inputs, the neural activity will eventually stay in this region $[D, B]$; (2) The

neural dynamic system is stable in the Lyapunov sense. We use the BIN technique to address the velocity jump problem in backstepping control. This method helps to eliminate the challenges and provides smooth velocity commands.

Replacing $A_i = A$, $B_i = B$, $D_i = D$, $x_i = \beta_i$, $S_i^+(t) = f_{1i}(\tilde{\theta}_i)$, $S_i^-(t) = g_{1i}(\tilde{\theta}_i)$ in (21), we can get

$$\dot{\beta}_i = -A\beta_i + (B - \beta_i)\, f_{1i}\left(\tilde{\theta}_i\right) - (D + \beta_i)\, g_{1i}\left(\tilde{\theta}_i\right). \tag{22}$$

Similarly, replacing $A_i = A$, $B_i = B$, $D_i = D$, $x_i = \gamma_i$, $S_i^+(t) = f_{2i}(\tilde{\theta}_i)$, $S_i^-(t) = g_{2i}(\tilde{\theta}_i)$ in (21), we can obtain

$$\dot{\gamma}_i = -A\gamma_i + (B - \gamma_i)\, f_{2i}\left(\tilde{\theta}_i\right) - (D + \gamma_i)\, g_{2i}\left(\tilde{\theta}_i\right), \tag{23}$$

where $f_{1i}(\tilde{\theta}_i)$, $g_{1i}(\tilde{\theta}_i)$, $f_{2i}(\tilde{\theta}_i)$ and $g_{2i}(\tilde{\theta}_i)$ are defined as

$$f_{1i}\left(\tilde{\theta}_i\right) = \max\left\{\frac{k_2}{k_3}\tilde{\theta}_i, 0\right\}, g_{1i}\left(\tilde{\theta}_i\right) = \max\left\{-\frac{k_2}{k_3}\tilde{\theta}_i, 0\right\}, \tag{24}$$

$$f_{2i}\left(\tilde{\theta}_i\right) = \max\left\{\frac{k_5}{k_6\sqrt{Y+1}}\tilde{\theta}_i, 0\right\}, g_{2i}\left(\tilde{\theta}_i\right) = \max\left\{-\frac{k_5}{k_6\sqrt{Y+1}}\tilde{\theta}_i, 0\right\}. \tag{25}$$

where k_2, k_3, k_5 and k_6 are positive constants.

4.2 Tracking control algorithm

We design a distributed formation control law to accomplish formation objectives (4) and (5) by utilizing the neighborhood formation tracking error and the leader's estimated state. The control law is designed using a combination of a BIN approach and a backstepping model. By replacing the variable $\tilde{\theta}_i$ in equation (22) with β_i, we obtain the proposed formation control law for each follower agent.

$$\begin{aligned} v_i &= v_{ir}\cos\tilde{\theta}_i + k_1{\alpha_1}^T R\left(\theta_i\right) e_i, \\ \omega_i &= k_2\beta_i + \dot{\theta}_{ir} + k_3\frac{\sin\tilde{\theta}_i}{\tilde{\theta}_i} v_{ir}{\alpha_2}^T R\left(\theta_i\right) e_i, \end{aligned} \tag{26}$$

where k_1, k_2, and k_3 are positive control gains, and α_1, α_2 are constant vectors given by $\alpha_1 = [1, 0]^T$ and $\alpha_2 = [0, 1]^T$.

It is evident from equation (22) that the value of β_i relies on the tracking error $\tilde{\theta}_i$, and as the input state changes, so does the shunting neural dynamic model's output state. The shunting model is dynamic in nature, and thus, the proposed control law (26) is a smooth function. This ensures that the output state of the shunting neural dynamic model changes gradually without any abrupt jumps, even in cases of abrupt input changes.

Remark 3 The control laws (26) have a similar structure to the tracking controllers in [17]. However, there are two main differences: (1) instead of the actual leader states v_r, $\dot{\theta}_r$, the estimated leader states v_{ir}, $\dot{\theta}_{ir}$ are used; and (2) the control law is developed using the followers' coordination error $p_j - p_i + \Delta_{ij}$ and the tracking error $\tilde{p}_i$. In this way, each follower robot does not need to know the leader's full state. The reliance on the state estimation of the leader is reduced, and the decentralization of the control is enhanced.

In the following, in order to facilitate the stability analysis, we define

$$s_i = \sum_{j=1}^{n} a_{ij}\tilde{p}_{ij} + b_i\tilde{p}_i. \tag{27}$$

Thus, e_i given in (18) can be expressed as

$$e_i = s_i + \sum_{j=1}^{n} a_{ij} \left(p_{jr} - p_{ir} \right). \tag{28}$$

Substituting (26) into (17), the closed-loop system becomes

$$\dot{\tilde{p}}_i = - k_1 R^T (\theta_i) \alpha_1 {\alpha_1}^T R (\theta_i) s_i + R^T (\theta_i) \alpha_2 v_{ir} \sin \tilde{\theta}_i + m_{1i}, \tag{29}$$

$$\dot{\tilde{\theta}}_i = - k_2 \beta_i - k_3 \frac{\sin \tilde{\theta}_i}{\tilde{\theta}_i} v_{ir} {\alpha_2}^T R (\theta_i) s_i + n_{1i}, \tag{30}$$

where $m_{1i} \in R^{2\times 2}$ and $n_{1i} \in R^{2\times 2}$ are calculated using

$$m_{1i} = \varrho_i - k_1 R^T (\theta_i) \alpha_1 {\alpha_1}^T R (\theta_i) \sum_{j=1}^{n} a_{ij} \left(p_{jr} - p_{ir} \right) \tag{31}$$

$$n_{1i} = -k_3 \frac{\sin \tilde{\theta}_i}{\tilde{\theta}_i} v_{ir} {\alpha_2}^T R (\theta_i) \sum_{j=1}^{n} a_{ij} \left(p_{jr} - p_{ir} \right). \tag{32}$$

4.3 Stability analysis

This part will discuss stability conditions using the Lyapunov functional technique. A technical lemma for the analysis of closed-loop system stability is proposed before the main conclusions.

Lemma 1 [37] For a continuously differentiable function $V : \mathbb{R}^+ \to \mathbb{R}^+$ and a uniformly continuous function $W : \mathbb{R}^+ \to \mathbb{R}^+$, if they satisfy the following condition for any $t \geq 0$

$$\dot{V}(t) \leq -W(t) + p_1(t)V(t) + p_2(t)\sqrt{V(t)}, \tag{33}$$

where $p_1(t)$ and $p_2(t)$ are nonnegative functions in L_1 space, and V (t) is bounded, then there is a constant c, so that as $t \to \infty$, $W(t) \to 0$ and $V(t) \to c$.

The primary result is now expressed as follows.

Theorem 1 Under Assumptions 1 and 2, the closed-loop systems (29) and (30) are asymptotically stable with the distributed estimator (6) and the formation controllers (26) by choosing the appropriate control gains k_1, k_2, and k_3; therefore, Problem 1 can be solved.

Proof. Consider the Lyapunov function candidate

$$V_3 = \frac{1}{2} \sum_{i=1}^{n} \left(\frac{1}{2} \sum_{j=1}^{n} a_{ij} \tilde{p}_{ij}^T \tilde{p}_{ij} + b_i \tilde{p}_i^T \tilde{p}_i + \frac{1}{k_3} \tilde{\theta}_i^2 + \frac{1}{B} {\beta_i}^2 \right). \tag{34}$$

The $\dot{V}_3$ along (29) and (30) is

$$\begin{aligned}\dot{V}_3 &= \sum_{i=1}^{n}\left(s_i{}^T\dot{\tilde{p}}_i + \frac{1}{k_3}\tilde{\theta}_i\dot{\tilde{\theta}}_i + \frac{1}{B}\beta_i\dot{\beta}_i\right)\\ &= \sum_{i=1}^{n}\left(-k_1 s_i{}^T R^T(\theta_i)\,\alpha_1\alpha_1{}^T R(\theta_i)\,s_i\right) + \sum_{i=1}^{n}\left(s_i{}^T R^T(\theta_i)\,\alpha_2 v_{ir}\sin\tilde{\theta}_i\right)\\ &\quad + \sum_{i=1}^{n}\left(-\frac{k_2}{k_3}\tilde{\theta}_i\beta_i - \sin\tilde{\theta}_i v_{ir}\alpha_2{}^T R(\theta_i)\,s_i\right) + \sum_{i=1}^{n}\left(s_i{}^T m_{1i}\right) + \sum_{i=1}^{n}\left(\frac{1}{k_3}\tilde{\theta}_i n_{1i}\right)\\ &\quad + \frac{1}{B}\sum_{i=1}^{n}\left(-A\beta_i{}^2 - f_{1i}(\tilde{\theta}_i)\,\beta_i{}^2 - g_{1i}(\tilde{\theta}_i)\,\beta_i{}^2\right) + \frac{1}{B}\sum_{i=1}^{n}\left(Bf_{1i}(\tilde{\theta}_i)\,\beta_i - Dg_{1i}(\tilde{\theta}_i)\,\beta_i\right).\end{aligned} \tag{35}$$

Then, we have by set $B = D$

$$\begin{aligned}\dot{V}_3 &= \sum_{i=1}^{n}\left(-k_1 s_i{}^T R^T(\theta_i)\,\alpha_1\alpha_1{}^T R(\theta_i)\,s_i\right)\\ &\quad + \frac{1}{B}\sum_{i=1}^{n}\left(-A - f_{1i}(\tilde{\theta}_i) - g_{1i}(\tilde{\theta}_i)\right)\beta_i{}^2 + \sum_{i=1}^{n}\left(f_{1i}(\tilde{\theta}_i) - g_{1i}(\tilde{\theta}_i) - \frac{k_2}{k_3}\tilde{\theta}_i\right)\beta_i\\ &\quad + \sum_{i=1}^{n}\left(s_i{}^T m_{1i}\right) + \sum_{i=1}^{n}\left(\frac{1}{k_3}\tilde{\theta}_i n_{1i}\right).\end{aligned} \tag{36}$$

According to $f_{1i}(\tilde{\theta}_i)$ and $g_{1i}(\tilde{\theta}_i)$ in (24), whenever $\tilde{\theta}_i \geq 0$ or $\tilde{\theta}_i < 0$, we can get

$$f_{1i}(\tilde{\theta}_i) - g_{1i}(\tilde{\theta}_i) - \frac{k_2}{k_3}\tilde{\theta}_i = 0. \tag{37}$$

Hence, equation (36) becomes

$$\dot{V}_3 = W_1 + W_2, \tag{38}$$

where W_1, W_2 are denoted as

$$W_1 = \sum_{i=1}^{n}\left(-k_1 s_i{}^T R^T(\theta_i)\,\alpha_1\alpha_1{}^T R(\theta_i)\,s_i\right) + \frac{1}{B}\sum_{i=1}^{n}\left(-A - f_{1i}(\tilde{\theta}_i) - g_{1i}(\tilde{\theta}_i)\right)\beta_i{}^2, \tag{39}$$

$$W_2 = \sum_{i=1}^{n}\left(s_i{}^T m_{1i}\right) + \sum_{i=1}^{n}\left(\frac{1}{k_3}\tilde{\theta}_i n_{1i}\right). \tag{40}$$

We can get $f_{1i}(\tilde{\theta}_i) \geq 0$ and $g_{1i}(\tilde{\theta}_i) \geq 0$ from (24). Furthermore, A and B are nonnegative constants. Thus, we have

$$\frac{1}{B}\left(-A - f_{1i}(\tilde{\theta}_i) - g_{1i}(\tilde{\theta}_i)\right)\beta_i{}^2 \leq 0. \tag{41}$$

We obtain that s_i denoted by (27) satisfies the following via the Cauchy-Schwarz inequality

$$\|s_i\|_2^2 \leq (n+1)\max_{0\leq j\leq n} a_{ij}\left(\sum_{j=1}^{n} a_{ij}\tilde{p}_{ij}^T\tilde{p}_{ij} + a_{i0}\tilde{p}_i^T\tilde{p}_i\right), \tag{42}$$

and the Lyapunov function V_3 can be demonstrated to satisfy

$$V_3 \geq \frac{1}{4}\sum_{i=1}^{n}\left(\sum_{j=1}^{n} a_{ij}\tilde{p}_{ij}^T\tilde{p}_{ij} + a_{i0}\tilde{p}_i^T\tilde{p}_i\right). \tag{43}$$

One can derive the inequality as follows

$$\sum_{i=1}^{n} \|s_i\|_2 \leq \sqrt{h_1 V_3}, \tag{44}$$

where $h_1 = 4(n+1) \max_{1\leq i\leq n, 1\leq j\leq n} \{a_{ij}\}$. Similarly, applying the Cauchy-Schwarz inequality with respect to $\tilde{\theta}_i$ can obtain $\left(\sum_{i=1}^{n} \left|\tilde{\theta}_i\right|\right)^2 \leq n \sum_{i=1}^{n} \tilde{\theta}_i^2$, and along with the fact $V_3 \geq \frac{1}{2k_3} \sum_{i=1}^{n} \tilde{\theta}_i^2$, we can get

$$\sum_{i=1}^{n} \left|\tilde{\theta}_i\right| \leq \sqrt{2nk_3 V_3}. \tag{45}$$

Using inequalities (44) and (45), we have

$$W_2 \leq \left(\max_{0\leq i\leq n} \|m_{1i}\|_2 \sqrt{h_1} + \max_{0\leq i\leq n} |n_{1i}| \sqrt{2n/k_3}\right) \sqrt{V_3}. \tag{46}$$

Since $[x_{ir}, y_{ir}, \theta_{ir}, v_{ir}, \omega_{ir}]$ asymptotically converges to the leader's state $[x_r, y_r, \theta_r, v_r, \omega_r]$, respectively, it can be verified that both $\|m_{1i}\|_2$ and $|n_{1i}|$ asymptotically converge to zero. Therefore, the Lyapunov function candidate V_3 satisfies Lemma 2's requirements, and we can obtain that W_1 tends to zero, or

$$\lim_{t\to 0} {\alpha_1}^T R(\theta_i(t)) s_i(t) = 0, \tag{47}$$

$$\lim_{t\to 0} \beta_i(t) = 0. \tag{48}$$

By applying Barbalat's lemma to (30), and considering that $\tilde{\theta}_i$ tends to zero, along with the facts that $\lim_{t\to 0} \frac{\sin\tilde{\theta}_i}{\tilde{\theta}_i} = 1$ and $\lim_{t\to 0} |v_r(t)| \geq 0$ by Assumption1, we have

$$\lim_{t\to 0} {\alpha_2}^T R(\theta_i(t)) s_i(t) = 0. \tag{49}$$

Combining (47) and (49), we can get

$$\lim_{t\to 0} s_i(t) = 0. \tag{50}$$

Denote $s = \left[{s_1}^T, {s_2}^T, \cdots, {s_n}^T\right]$ and $\tilde{p} = \left[\tilde{p}_1^T, \tilde{p}_2^T, \cdots, \tilde{p}_n^T\right]$, and given $s = H\tilde{p}$ as denoted by (27). Thus, following (50), we can get

$$\lim_{t\to 0} \tilde{p}(t) = 0. \tag{51}$$

Since the formation tracking error $\tilde{p}_i$ and $\tilde{\theta}_i$ asymptotically converge to zero, we can achieve the control goals (4) and (5). This completes the proof.

5. SATURATED VELOCITIES FORMATION TRACKING CONTROLLER DESIGN

Since the velocities of nonholonomic multiagents are limited, it is necessary to take the control input saturation into account. Therefore, in order to prevent saturation velocities from causing input saturation, it is essential to develop a formation controller with saturation velocities for each follower agent i to guarantee that v_i and ω_i satisfy

$$|v_i(t)| \leq v_i^{\max}, \quad |\omega_i(t)| \leq \omega_i^{\max}, \quad \forall t \geq 0, \tag{52}$$

where $v_i^{\max}$ and $\omega_i^{\max}$ is the maximum of the velocity.

Furthermore, to ensure the feasibility of formation implementation, the leader's velocity v_r and ω_r should be given to satisfy $v_i^{\max} > v_r^{\max}, \omega_i^{\max} > \omega_r^{\max}$.

Inspired by a BIN approach and backstepping model, the design of a saturated velocities constrained formation tracking controller for follower agents is as follows

$$v_i = v_{ir}\cos\tilde{\theta}_i + \frac{k_4{\alpha_1}^T R\left(\theta_i\right)e_i}{\sqrt{X+1}},$$
$$\omega_i = \frac{k_5\gamma_i}{\sqrt{Y+1}} + \dot{\theta}_{ir} + \frac{k_6\frac{\sin\tilde{\theta}_i}{\tilde{\theta}_i}v_{ir}{\alpha_2}^T R\left(\theta_i\right)e_i}{\sqrt{X+1}}, \tag{53}$$

where k_4 k_5 and k_6 are positive control gains, $X = \sum_{j=1}^{n} a_{ij}\tilde{p}_{ij}^T\tilde{p}_{ij} + b_i\tilde{p}_i^T\tilde{p}_i$ and $Y = {\gamma_i}^2$. Substituting (53) into (17), the closed-loop system becomes

$$\dot{\tilde{p}}_i = \frac{-k_4R^T\left(\theta_i\right)\alpha_1{\alpha_1}^T R\left(\theta_i\right)s_i}{\sqrt{X+1}} + R^T\left(\theta_i\right)\alpha_2 v_{ir}\sin\tilde{\theta}_i + m_{2i}, \tag{54}$$
$$\dot{\tilde{\theta}}_i = \frac{-k_5\gamma_i}{\sqrt{Y+1}} - \frac{k_6\frac{\sin\tilde{\theta}_i}{\tilde{\theta}_i}v_{ir}{\alpha_2}^T R\left(\theta_i\right)s_i}{\sqrt{X+1}} + n_{2i}, \tag{55}$$

where $m_{2i} \in R^{2\times 2}$ and $n_{2i} \in R^{2\times 2}$ are given by

$$m_{2i} = \delta_i - \frac{k_4R^T\left(\theta_i\right)\alpha_1{\alpha_1}^T R\left(\theta_i\right)\sum_{j=1}^{n} a_{ij}\left(p_{jr}-p_{ir}\right)}{\sqrt{X+1}}, \tag{56}$$
$$n_{2i} = \frac{-k_6\frac{\sin\tilde{\theta}_i}{\tilde{\theta}_i}v_{ir}{\alpha_2}^T R\left(\theta_i\right)\sum_{j=1}^{n} a_{ij}\left(p_{jr}-p_{ir}\right)}{\sqrt{X+1}}. \tag{57}$$

Theorem 2 Under the formation tracking controller (53), the closed-loop systems (54) and (55) are asymptotically stable, and the formation control objectives (4) and (5) can be achieved. By selecting suitable gains k_4 k_5 and k_6, the control inputs v_i and ω_i satisfy the constraint (52).

Proof. Consider the Lyapunov function candidate

$$V_4 = \frac{1}{2}\sum_{i=1}^{n}\left(\frac{1}{2}(X+1)^{\frac{1}{2}} + \frac{1}{k_6}\tilde{\theta}_i^2 + \frac{1}{B}{\gamma_i}^2\right). \tag{58}$$

The $\dot{V}_4$ along (54) and (55) is

$$\begin{aligned}\dot{V}_4 &= \sum_{i=1}^{n}\left(\frac{{s_i}^T\dot{\tilde{p}}_i}{\sqrt{X+1}} + \frac{1}{k_6}\tilde{\theta}_i\dot{\tilde{\theta}}_i + \frac{1}{B}\gamma_i\dot{\gamma}_i\right)\\ &= \sum_{i=1}^{n}\left(\frac{-k_4{s_i}^T R^T\left(\theta_i\right)\alpha_1{\alpha_1}^T R\left(\theta_i\right)s_i}{X+1} + \frac{{s_i}^T R^T\left(\theta_i\right)\alpha_2 v_{ir}\sin\tilde{\theta}_i}{\sqrt{X+1}}\right) + \sum_{i=1}^{n}\left(-\frac{k_5}{k_6\sqrt{Y+1}}\tilde{\theta}_i\gamma_i - \frac{\sin\tilde{\theta}_i v_{ir}{\alpha_2}^T R\left(\theta_i\right)s_i}{\sqrt{X+1}}\right)\\ &\quad + \frac{1}{B}\sum_{i=1}^{n}\left(Bf_{2i}\left(\tilde{\theta}_i\right)\gamma_i - Dg_{2i}\left(\tilde{\theta}_i\right)\gamma_i\right) + \frac{1}{B}\sum_{i=1}^{n}\left(-A{\gamma_i}^2 - f_{2i}\left(\tilde{\theta}_i\right){\gamma_i}^2 - g_{2i}\left(\tilde{\theta}_i\right){\gamma_i}^2\right)\\ &\quad + \sum_{i=1}^{n}\left(\frac{{s_i}^T m_{2i}}{\sqrt{X+1}}\right) + \sum_{i=1}^{n}\left(\frac{1}{k_6}\tilde{\theta}_i n_{2i}\right).\end{aligned} \tag{59}$$

Then, we have by set $B = D$

$$\dot{V}_4 = \sum_{i=1}^{n}\left(\frac{-k_4 {s_i}^T R^T(\theta_i)\alpha_1{\alpha_1}^T R(\theta_i) s_i}{X+1}\right) + \frac{1}{B}\sum_{i=1}^{n}\left(-A - f_{2i}(\tilde{\theta}_i) - g_{2i}(\tilde{\theta}_i)\right){\gamma_i}^2 + \sum_{i=1}^{n}\left(f_{2i}(\tilde{\theta}_i) - g_{2i}(\tilde{\theta}_i) - \frac{k_5}{k_6\sqrt{Y+1}}\tilde{\theta}_i\right)\gamma_i + \sum_{i=1}^{n}\left(\frac{{s_i}^T m_{2i}}{\sqrt{X+1}}\right) + \sum_{i=1}^{n}\left(\frac{1}{k_6}\tilde{\theta}_i n_{2i}\right). \tag{60}$$

And according to $f_{2i}(\tilde{\theta}_i)$ and $g_{2i}(\tilde{\theta}_i)$ in (25), whenever $\tilde{\theta}_i \geq 0$ or $\tilde{\theta}_i < 0$, we can get

$$f_{2i}(\tilde{\theta}_i) - g_{2i}(\tilde{\theta}_i) - \frac{k_5}{k_6\sqrt{Y+1}}\tilde{\theta}_i = 0. \tag{61}$$

Hence, equation (60) becomes

$$\dot{V}_4 = W_3 + W_4, \tag{62}$$

where W_3 and W_4 are defined as

$$W_3 = \sum_{i=1}^{n}\left(\frac{-k_4 {s_i}^T R^T(\theta_i)\alpha_1{\alpha_1}^T R(\theta_i) s_i}{X+1}\right) + \frac{1}{B}\sum_{i=1}^{n}\left(-A - f_{2i}(\tilde{\theta}_i) - g_{2i}(\tilde{\theta}_i)\right){\gamma_i}^2, \tag{63}$$

$$W_4 = \sum_{i=1}^{n}\left(\frac{{s_i}^T m_{2i}}{\sqrt{X+1}}\right) + \sum_{i=1}^{n}\left(\frac{1}{k_6}\tilde{\theta}_i n_{2i}\right). \tag{64}$$

According to the functions of $f_{2i}(\tilde{\theta}_i)$ and $\mathbf{g}_{2i}(\tilde{\theta}_i)$ in (25), we have $f_{2i}(\tilde{\theta}_i) \geq 0$ and $g_{2i}(\tilde{\theta}_i) \geq 0$. Therefore, A and B are nonnegative constants. Thus, we can get

$$\frac{1}{B}\left(-A - f_{2i}(\tilde{\theta}_i) - g_{2i}(\tilde{\theta}_i)\right){\gamma_i}^2 \leq 0. \tag{65}$$

We obtain that s_i denoted by (27) satisfies the following via the Cauchy-Schwarz inequality

$$\|s_i\|_2^2 \leq (n+1)\max_{0\leq j\leq n} a_{ij}\left(\sum_{j=1}^{n} a_{ij}\tilde{p}_{ij}^T\tilde{p}_{ij} + a_{i0}\tilde{p}_i^T\tilde{p}_i\right) \tag{66}$$

and the Lyapunov function V_4 can be demonstrated to satisfy

$$V_4 \geq \frac{1}{4}\sum_{i=1}^{n}\sqrt{\left(\sum_{j=1}^{n} a_{ij}\tilde{p}_{ij}^T\tilde{p}_{ij} + a_{i0}\tilde{p}_i^T\tilde{p}_i\right)}. \tag{67}$$

One can derive the inequality as follows

$$\sum_{i=1}^{n}\|s_i\|_2 \leq h_2 V_4, \tag{68}$$

where $h_2 = 4\sqrt{(n+1)\max_{1\leq i\leq n,1\leq j\leq n}\{a_{ij}\}}$. Similarly, applying the Cauchy-Schwarz inequality with respect to $\tilde{\theta}_i$ can obtain $\left(\sum_{i=1}^{n}\left|\tilde{\theta}_i\right|\right)^2 \leq n\sum_{i=1}^{n}\tilde{\theta}_i^2$, and based on the fact $V_4 \geq \frac{1}{2k_6}\sum_{i=1}^{n}\tilde{\theta}_i^2$, we get

$$\sum_{i=1}^{n}\left|\tilde{\theta}_i\right| \leq \sqrt{2nk_6 V_4}. \tag{69}$$

Using inequalities (68) and (69), we have

$$W_4 \leq \left(\max_{0\leq i\leq n}\frac{\|m_{2i}\|_2}{\sqrt{X+1}}\sqrt{h_2}\right)V_4 + \left(\max_{0\leq i\leq n}|n_{2i}|\sqrt{2n/k_6}\right)\sqrt{V_4}. \tag{70}$$

Since $[x_{ir}, y_{ir}, \theta_{ir}, v_{ir}, \omega_{ir}]$ asymptotically converges to the leader's state $[x_r, y_r, \theta_r, v_r, \omega_r]$ respectively, it can be verified that both $\|m_{2i}\|_2$ and $|n_{2i}|$ asymptotically converge to zero. Therefore, the Lyapunov function V_4 satisfies Lemma 2's requirements and we can obtain that W_3 tends to zero, or

$$\lim_{t\to 0} {\alpha_1}^T R\left(\theta_i\left(t\right)\right) s_i\left(t\right) = 0, \tag{71}$$

$$\lim_{t\to 0} \gamma_i\left(t\right) = 0. \tag{72}$$

Using Barbalat's lemma to (55), since $\tilde{\theta}_i$ tends to zero and the facts that $\lim_{t\to 0} \frac{\sin\tilde{\theta}_i}{\tilde{\theta}_i} = 1$ and $\lim_{t\to 0} |v_r\left(t\right)| \geq 0$ by Assumption 1, we have

$$\lim_{t\to 0} {\alpha_2}^T R\left(\theta_i\left(t\right)\right) s_i\left(t\right) = 0. \tag{73}$$

Combining (71) and (73), we can get

$$\lim_{t\to 0} s_i\left(t\right) = 0. \tag{74}$$

Denote $s = \left[{s_1}^T, {s_2}^T, \cdots, {s_n}^T\right]$ and $\tilde{p} = \left[\tilde{p}_1^T, \tilde{p}_2^T, \cdots, \tilde{p}_n^T\right]$, and given $s = H\tilde{p}$ as denoted by (27). Thus, following (74), we can get

$$\lim_{t\to 0} \tilde{p}\left(t\right) = 0. \tag{75}$$

The formation tracking errors $\tilde{p}_i$ and $\tilde{\theta}_i$ asymptotically converge to zero; thus, we can achieve the control goals (4) and (5).

Subsequently, by letting k_4 k_5 and k_6 satisfy the following inequations

$$|v_i\left(t\right)| \leq v_r^{\max} + k_4 \leq v_i^{\max}, \tag{76}$$

$$|\omega_i\left(t\right)| \leq k_5 + \omega_r^{\max} + k_6 v_r^{\max} \leq \omega_i^{\max} \qquad \forall t \geq 0, \tag{77}$$

v_i and ω_i meet the constraints in (52), avoiding input saturation caused by the saturation velocity. The proof is completed.

Remark 1 Indeed, the constrained controller (53) constructs the nonlinear dynamic gain by dividing by a few positive error terms, such as $\sqrt{\sum_{j=1}^{n} a_{ij}\tilde{p}_{ij}^T\tilde{p}_{ij} + b_i\tilde{p}_i^T\tilde{p}_i + 1}$, and $\sqrt{{\gamma_i}^2 + 1}$, so that the structure of this controller is similar to the unconstrained controller (26). Even though the unconstrained controller (26) can also change the gain to prevent input saturation due to the saturation velocities, it has the disadvantages of lack of flexibility and inconvenience. On the one hand, the nonlinear dynamic gain of the constrained controller (53) is relatively small compared with the unconstrained controller (26) with higher gain to guarantee v_i and ω_i do not exceed the maximum speed $v_i^{\max}$ and $\omega_i^{\max}$ of the follower. On the other hand, the nonlinear dynamic gain of the constrained controller (53) is relatively larger and the convergence time is shorter compared to the unconstrained controller (26) with lower gain.

6. NUMERICAL SIMULATIONS

Several simulations are presented in this section to validate the effectiveness and feasibility of the distributed estimator and formation control law. In the first part, since the estimation term will be used in the formation controller, for the unconstrained formation controller (UFC) (26), we confirm the validity of the estimator. Then, we will prove the validity of the UFC. In the second part, we demonstrate the effectiveness of the velocity constrained formation controller (CFC) (53). Then, two groups of parameters for the UFC (26) are chosen: one is a group of higher gains to achieve that the convergence time of formation errors under the UFC (26) is basically consistent with that under the CFC (53); the other is a group of lower gains to ensure that the control input amplitudes under the UFC (26) are at the same levels as the control input amplitudes under the CFC

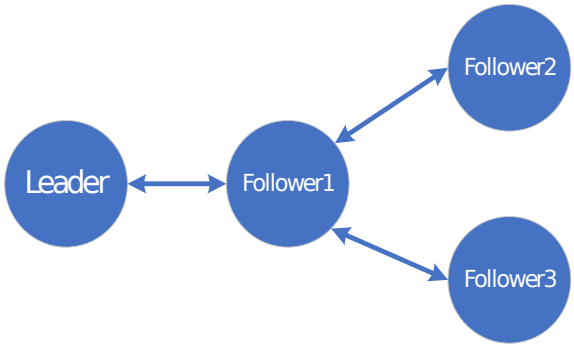

Figure 2. Communication topology graph between one leader and three followers.

Table 1. Adjustment time of tracking errors (SEC)

Tracking error	$x_r - x_2 + \Delta_{2x}$	$y_r - y_2 + \Delta_{2y}$	$\theta_r - \theta_2$
Controller(26) (Higher gains)	9.60	12.80	8.70
Controller(54)	9.22	12.34	6.33
Controller(26) (Lower gains)	9.65	15.45	10.97
Controller(80)	19.36	16.74	16.71

(53). At the same time, compared with another saturated velocity formation controller (SFC) proposed in [34], the superiority of the velocity CFC proposed in this paper is proved.

6.1 Unconstrained controller

Consider the communication link for a leader agent and three follower agents, as shown in Figure 2. The leader's linear velocities and the angular velocities are set as $v_0 = 2 - 0.5cos(t)$ and $\omega_0 = 0.5cos(t)$. The initial state values of the three followers and one leader are $(x_1, y_1, \theta_1) = (1.5, 2, 0,)$, $(x_2, y_2, \theta_2) = (0, 3, -0.5)$, $(x_3, y_3, \theta_3) = (0, 0, -1)$ and $(x_0, y_0, \theta_0) = (2, 2.5, 0.6)$. Moreover, desired relative positions are $\Delta_{1x} = -2, \Delta_{2x} = -4, \Delta_{3x} = 4, \Delta_{1y} = 4, \Delta_{2y} = 2, \Delta_{3y} = -2$ for each robot i. The parameters are chosen in estimation laws $\sigma_1 = 5, \sigma_2 = 2$. Similarly, the parameters chosen for control law are chosen to be $k_1 = 1$, $k_2 = 2.5$, $k_3 = 0.5$, $A = 5$, $B = 1$, and $D = 1$. Then, by exploiting the estimator (6), Figures 3 and 4 demonstrate that the estimation errors $(x_{ir} - x_r)$, $(y_{ir} - y_r)$, $(\theta_{ir} - \theta_r)$ and $(v_{ir} - v_r)$, $(\omega_{ir} - \omega_r)$ converge to zero. Furthermore, Figures 5-8 display the simulation of the UFC (26) using this estimation term. It is evident from Figure 5 that the three follower robots guided by the leader robot form the desired triangular formation in a certain time, and in Figure 6, the position and orientation tracking errors converge to zero; i.e., the control objectives (4) and (5) are achieved. Figures 7 and 8 depict the evolution of linear velocities and angular velocities of one leader and three follower agents. It is evident that all three of the following agents will ultimately be able to match the leader agent's angular and linear velocities.

6.2 Constrained controller

Define the following formation tracking errors as

$$\begin{bmatrix} x_{ei} \\ y_{ei} \\ \theta_{ei} \end{bmatrix} = \begin{bmatrix} \cos\theta_i & \sin\theta_i & 0 \\ -\sin\theta_i & \cos\theta_i & 0 \\ 0 & 0 & 1 \end{bmatrix} \begin{bmatrix} x_{ir} - x_i + \Delta_{ix} \\ y_{ir} - y_i + \Delta_{iy} \\ \theta_{ir} - \theta_i \end{bmatrix}.$$

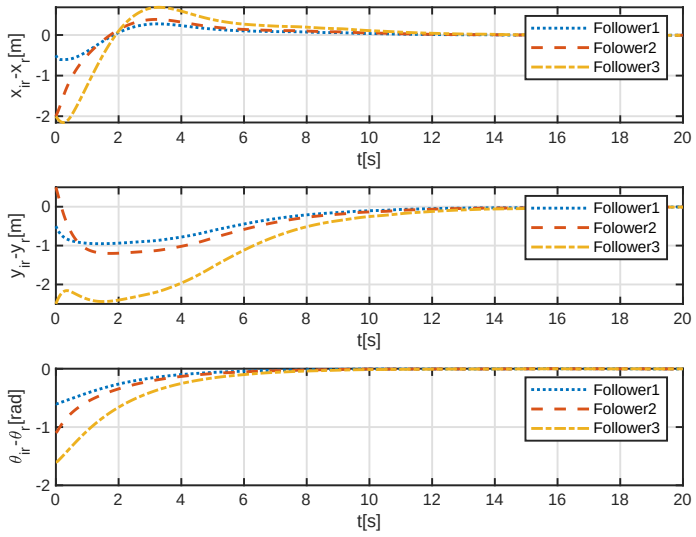

Figure 3. Estimation error $(x_{ir} - x_r)$, $(y_{ir} - y_r)$ and $(\theta_{ir} - \theta_r)$.

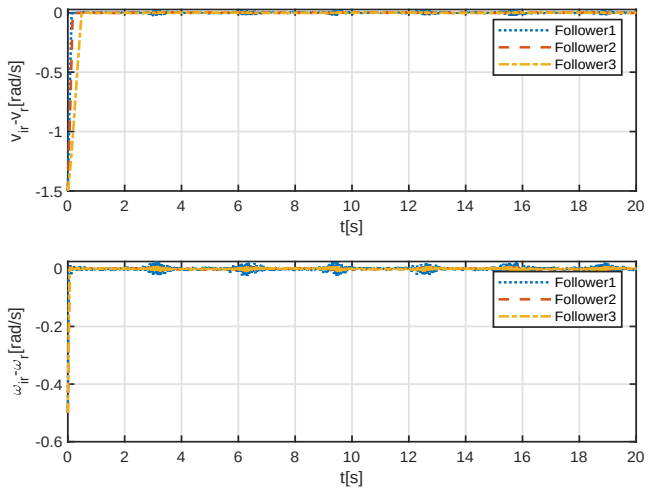

Figure 4. Estimation error $(v_{ir} - v_r)$ and $(\omega_{ir} - \omega_r)$.

Based on the above formation tracking errors, a constrained formation tracking controller with saturated velocities for the follower agents is given as

$$
\begin{aligned}
v_i &= v_{ir} + \frac{k_7 x_{ei}}{\sqrt{x_{ei}^2 + y_{ei}^2 + 1}}, \\
\omega_i &= \omega_{ir} + \frac{k_8 \sin\frac{\theta_{ei}}{2}}{\sqrt{x_{ei}^2 + y_{ei}^2 + 1}} + \frac{k_9 v_{ir}(y_{ei}\cos\frac{\theta_{ei}}{2} - x_{ei}\sin\frac{\theta_{ei}}{2})}{\sqrt{x_{ei}^2 + y_{ei}^2 + 1}}
\end{aligned} \tag{78}
$$

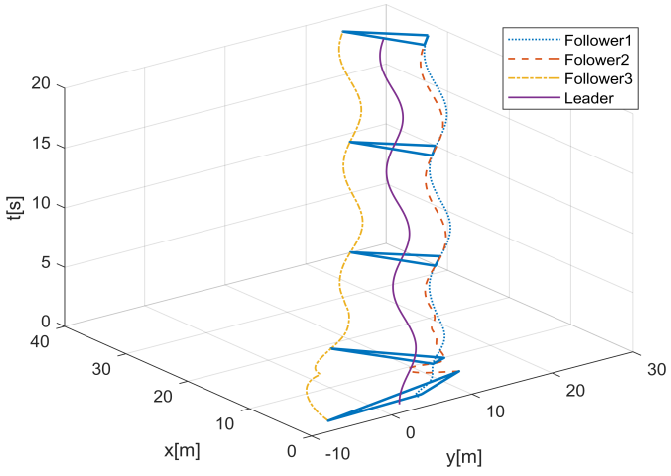

Figure 5. The evolution trajectory of one leader and three follower robots' position in the (x, y, t) plane.

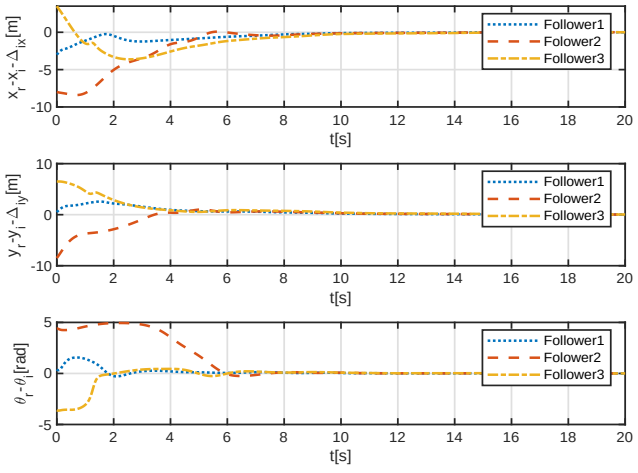

Figure 6. Evolution of position and orientation tracking error.

where k_7, k_8, and k_9 are positive gains and satisfy the following

$$|v_i(t)| \leq v_r^{\max} + k_7 \leq v_i^{\max}, \tag{79}$$

$$|\omega_i(t)| \leq k_8 + \omega_r^{\max} + 2k_9 v_r^{\max} \leq \omega_i^{\max} \qquad \forall t \geq 0, \tag{80}$$

The velocity constraints are defined as $v_i \in [-4, 4]$ and $\omega_i \in [-3.5, 3.5]$. The group reference velocities have bounds of $v_r^+ = 2.5$, $v_r^- = 1.5$, and $\omega_r^+ = 0.5$, $\omega_r^- = -0.5$. The leader's linear velocities and the angular velocities are set as $v_0 = 2 - 0.5cos(t)$ and $\omega_0 = 0.5cos(t)$, which satisfy Assumptions 2. Based on (76) and (77), adjust the control law parameters $k_4 = 1.5$, $k_5 = 6.8$, $k_6 = 0.6$, $A = 8$, $B = 1$, $D = 0.2$. The leaders' initial state value is considered as $(x_0, y_0, \theta_0) = (2, 2.5, 0.6)$. Moreover, desired relative positions are $\Delta_{1x} = -2, \Delta_{2x} = -4, \Delta_{3x} = 4, \Delta_{1y} = 4, \Delta_{2y} = 2, \Delta_{3y} = -2$ for each robot i. For CFC (53), Figure 9 displays the path of all mobile robots during the 0-20 s, indicating that they converge to the desired formation. Figure 10 demonstrates that the formation tracking errors converge to zero, thereby achieving objectives (4) and (5).

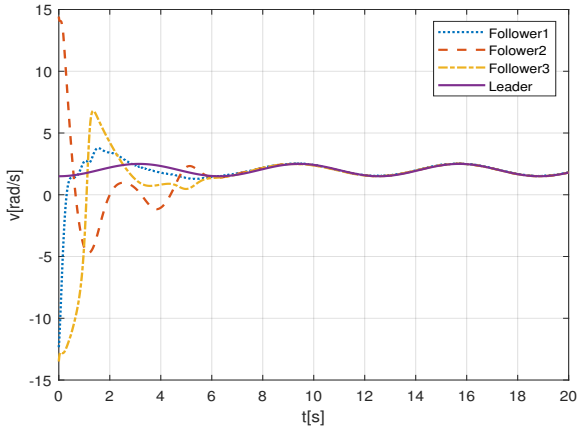

Figure 7. Evolution of position and orientation tracking error.

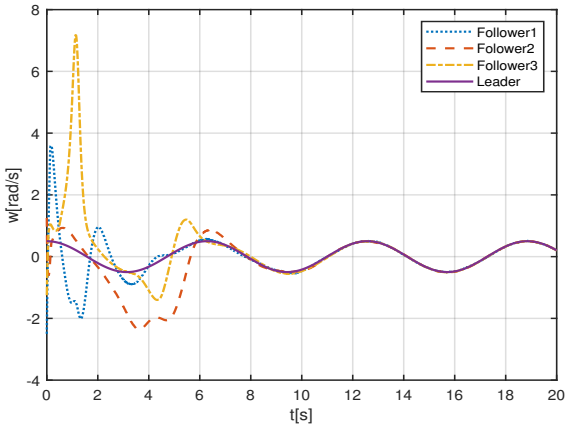

Figure 8. Evolution of angular velocity of one leader and three follower agents.

Then, we choose Follower 2 as the comparison object. The higher gains of the UFC (26) are taken as $k_1 = 2$, $k_2 = 4$, and $k_3 = 1$, and the lower gains of the UFC (26) are taken as $k_1 = 0.7$, $k_2 = 1$, and $k_3 = 0.2$. The gains of the CFC (53) are taken as $k_4 = 1.5$, $k_5 = 6.8$, and $k_6 = 0.6$. The gains of the SFC (78) are taken as $k_7 = 0.7$, $k_8 = 2.5$, and $k_9 = 1.5$. The rule of parameter selection for the SFC (78) is to make the response curves of formation errors obtain better dynamic and steady-state performance as far as possible under the premise that the gains k_7, k_8, and k_9 meet the constraints in (79) and (80) while comparing. Figures 11-13 show the status errors of follower 2 respectively. The curve of the control input is depicted in Figures 14 and 15. For a clearer comparison of the performance of the various controllers, tracking error adjustment times are listed in Table 1.

According to Table 1, Figures 14 and 15, the tracking error convergence time of UFC (26) with a higher gain is almost the same as that of CFC (53), but CFC (53) is effective against input saturation and can keep the maximum linear velocity and angular velocity not exceeding the threshold. The tracking error convergence time of the CFC (53) is shorter than that of the UFC (26) with lower gain while ensuring the same control input amplitude. In addition, through simulation comparison, both CFC (53) and SFC (78) satisfy the velocity constraint in equation (52), and CFC (53) guarantees better dynamic performance than controller (78).

According to the above simulation results, compared with UFC (26) and SFC (78), CFC (53) ensures that the

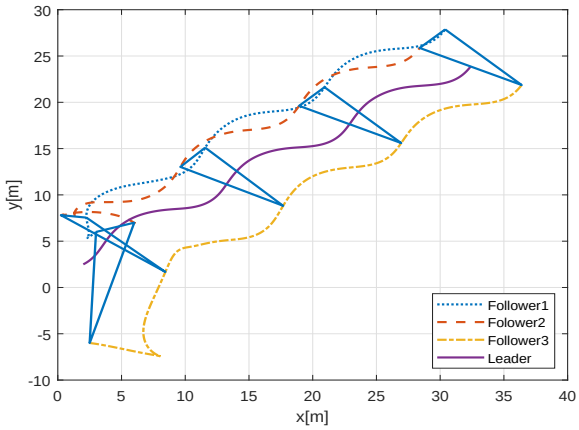

Figure 9. The evolution trajectory of one leader and three follower agents' position in the (x, y) plane.

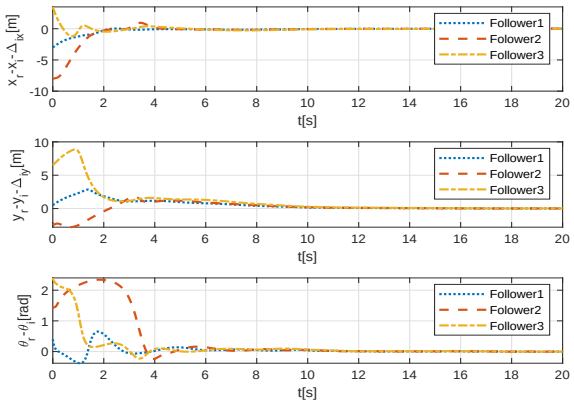

Figure 10. Evolution of position and orientation tracking error.

control input meets the saturation constraint and does not lead to a significant increase in adjustment time. At the same time, it is obvious that the convergence time of the UFC (26) is much smaller than that of the SFC (78) regardless of whether the parameters of the UFC (26) are chosen as high or low gain. The superiority of the proposed controller is demonstrated.

7. CONCLUSION

By employing a BIN approach, this study addresses the issue of leader-following formation control for a group of nonholonomic multiagents. For each follower, a distributed estimator is designed to estimate the leaders' state information. Based on the distributed estimator, we propose backstepping-based unconstrained and saturated velocity CFCs, respectively. We also introduce BIN modeling to address the problem of impractical velocity jumps, allowing the follower agent to maintain the desired geometry without relying on the leader's state information. Furthermore, sufficient conditions for constructing candidate sets of Lyapunov functionals are given. Simulation results confirm that the proposed control law is effective. The method proposed in this paper is based on an undirected graph and has some limitations. In future work, the proposed method will be extended to directed graphs and the collision and obstacle avoidance problems in the formation control of nonholonomic multiagent systems will be considered. At the same time, extending the kinematic control to

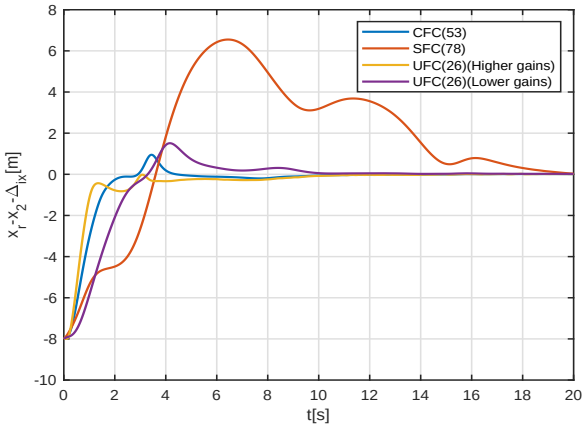

Figure 11. Time evolution histories of $x_r - x_2 + \Delta_{2x}$ of follower2.

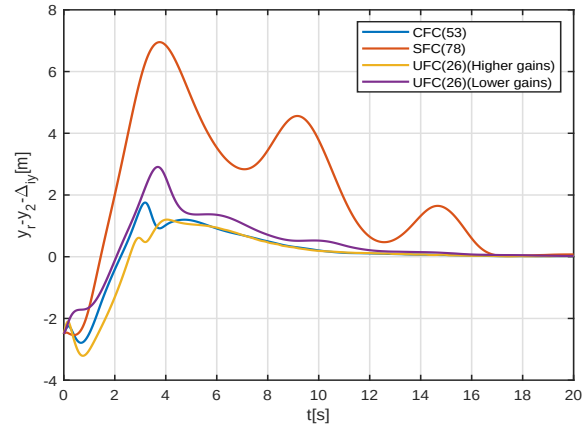

Figure 12. Time evolution histories of $y_r - y_2 + \Delta_{2y}$ of follower2.

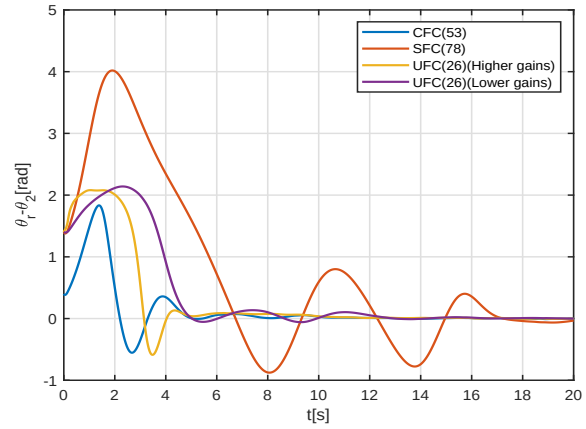

Figure 13. Time evolution histories of $\theta_r - \theta_2$ of follower2.

the dynamic level is also a direction of effort.

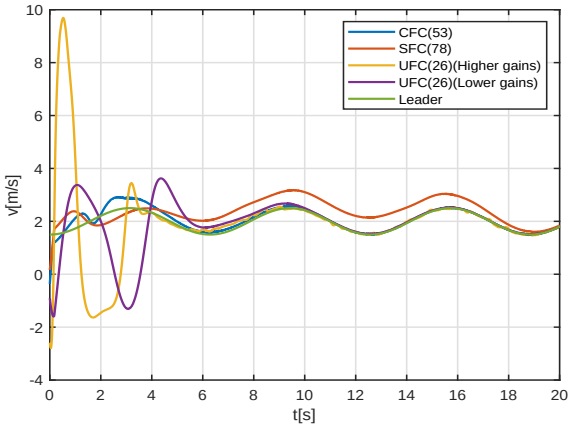

Figure 14. Time evolution histories of linear velocity of follower2.

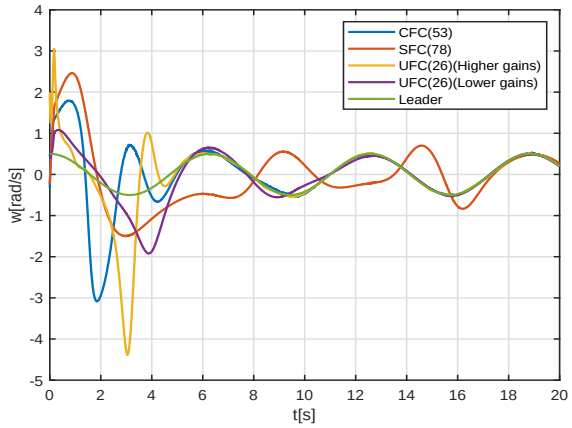

Figure 15. Time evolution histories of angular velocity of follower2.

DECLARATIONS

Authors' contributions

Made substantial contributions to conception and design of the study and performed data analysis and interpretation: Zhao XW, Li MK

Performed data acquisition and provided administrative, technical, and material support: Lai Q, Liu ZW

Availability of data and materials

Not applicable.

Financial support and sponsorship

The authors are grateful for the support of the National Natural Science Foundation of China under grant 62173121.

Conflicts of interest

Lai Q is a Junior Editorial Board Member of the journal *Intelligence & Robotics*, while the other authors have declared that they have no conflicts of interest.

Ethical approval and consent to participate

Not applicable.

Consent for publication

Not applicable.

Copyright

REFERENCES

1. Wu C, Fang H, Yang Q, Zeng X, Wei Y, Chen J. Distributed cooperative control of redundant mobile manipulators with safety constraints. *IEEE Trans Cybern* 2023;53:1195–207. DOI
2. Gabriel J, Deutscher J. Robust cooperative output regulation for networks of hyperbolic PIDE-ODE systems. *IEEE Trans Autom Control* 2024;69:888–903. DOI
3. Feng S, Li X, Ren L, Xu S. Reinforcement learning with parameterized action space and sparse reward for UAV navigation. *Intell Robot* 2023;3:161–75. DOI
4. Lv J, Wang C, Liu B, Kao Y, Jiang Y. Fully distributed prescribed-time consensus control of multiagent systems under fixed and switching topologies. *Inform Sci* 2023;648:119538. DOI
5. Zhao XW, Chi M, Guan ZH, Hu B, Zhang XH. Flocking of multiple three-dimensional nonholonomic agents with proximity graph. *J Franklin I* 2017;354:3617–33. DOI
6. Fu H, Chen X, Wang W, Wu M. Data-based optimal synchronization control for discrete-time nonlinear heterogeneous multiagent systems. *IEEE Trans Cybern* 2022;52:2477–90. DOI
7. Santilli M, Franceschelli M, Gasparri A. Secure rendezvous and static containment in multi-agent systems with adversarial intruders. *Automatica* 2022;143:110456. DOI
8. Zhang J, Fu Y, Fu J. Optimal formation control of second-order heterogeneous multiagent systems using adaptive predefined-time strategy. *IEEE Trans Fuzzy Syst* 2024;32:2390–402. DOI
9. Huang H, Savkin AV, Huang C. Decentralized autonomous navigation of a UAV network for road traffic monitoring. *IEEE Trans Aerosp Electron Syst* 2021;57:2558–64. DOI
10. Koung D, Kermorgant O, Fantoni I, Belouaer L. Cooperative multi-robot object transportation system based on hierarchical quadratic programming. *IEEE Trans Robot Autom Lett* 2021;6:6466–72. DOI
11. Kamel MA, Yu X, Zhang Y. Formation control and coordination of multiple unmanned ground vehicles in normal and faulty situations: a review. *Annu Rev Control* 2020;49:128–44. DOI
12. Zheng Z, Duan H. UAV maneuver decision-making via deep reinforcement learning for short-range air combat. *Intell Robot* 2023;3:76–94. DOI
13. Leng K, Li S. Distribution path optimization for intelligent logistics vehicles of urban rail transportation using VRP optimization model. *IEEE T Intell Transp* 2022;23:1661–9. DOI
14. Xie Y, Han L, Dong X, Li Q, Ren Z. Bio-inspired adaptive formation tracking control for swarm systems with application to UAV swarm systems. *Neurocomputing* 2021;453:272–85. DOI
15. Wang Y, Shan M, Yue Y, Wang D. Vision-based flexible leader-follower formation tracking of multiple nonholonomic mobile robots in unknown obstacle environments. *IEEE Trans Control Syst Technol* 2020;28:1025–33. DOI
16. Min X, Baldi S, Yu W. Funnel-based asymptotic control of leader–follower nonholonomic robots subject to formation constraints. *IEEE Trans Control Netw Syst* 2023;10:1313–25. DOI
17. Liu W, Wang X, Li S. Formation control for leader–follower wheeled mobile robots based on embedded control technique. *IEEE Trans Contr Syst Technol* 2023;31:265–80. DOI
18. Miao Z, Liu YH, Wang Y, Yi G, Fierro R. Distributed estimation and control for leader-following formations of nonholonomic mobile robots. *IEEE Trans Autom Sci Eng* 2018;15:1946–54. DOI
19. Zhang J, Yang D, Zhang H,Su H. Adaptive secure practical fault-tolerant output regulation of multiagent systems with DoS attacks by asynchronous communications. *IEEE Trans Netw Sci Eng* 2023;10:4046–55. DOI
20. Liu Y, Huang P, Zhang F, Zhao Y. Distributed formation control using artificial potentials and neural network for constrained multiagent systems. *IEEE Trans Control Syst Technol* 2020;28:697–704. DOI
21. Li Y, Dong S, Li K, Tong S. Fuzzy adaptive fault tolerant timevarying formation control for nonholonomic multirobot systems with range constraints. *IEEE Trans Intell Veh* 2023;8:3668–79. DOI
22. Fei Y, Shi P, Lim CC. Robust and collision-free formation control of multiagent systems with limited information. *IEEE Trans Neural Netw Learn Syst* 2023;34:4286–95. DOI
23. He W, Meng T, He X, Ge S. Unified iterative learning control for flexible structures with input constraints. *Automatica* 2018;96:326–36. DOI
24. Yin T, Gu Z, Xie X. Observer-based event-triggered sliding mode control for secure formation tracking of multi-UAV systems. *IEEE*

Trans Netw Sci Eng 2023;10:887–98. DOI
25. Soni, Kumar N. Backstepping based intelligent control of tractor-trailer mobile manipulators with wheel slip consideration. *ISA T* 2024;153:78–95. DOI
26. Zheng X, Yang X, Zhao H, Chen Y. Saturated adaptive-law-based backstepping and its applications to a quadrotor hover. *IEEE Trans Ind Electron* 2022;69:13473–82. DOI
27. Yan C, Xia J, Liu X, Yue H, Li C. Adaptive backstepping control of high-order fully actuated nonlinear systems with event-triggered strategy. *Intell Robot* 2023;3:176–89. DOI
28. Hodgkin AL, Huxley AF. A quantitative description of membrane current and its application to conduction and excitation in nerve. *J Physiol* 1952;117:500–44. DOI
29. Yang SX, Zhu A, Yuan G, Meng MQH. A bioinspired neurodynamics-based approach to tracking control of mobile robots. *IEEE Trans Ind Electron* 2012;59:3211-20. DOI
30. Pan CZ, Lai XZ, Yang SX, Wu M. A biologically inspired approach to tracking control of underactuated surface vessels subject to unknown dynamics. *Expert Syst Appl* 2015;42:2153–-61. DOI
31. Moorthy S, Joo YH. Distributed leader-following formation control for multiple nonholonomic mobile robots via bioinspired neurodynamic approach. *Neurocomputing* 2022;492:308–21. DOI
32. Ren W, Beard RW. Trajectory tracking for unmanned air vehicles with velocity and heading rate constraints. *IEEE Trans Control Syst Technol* 2004;12:706–16. DOI
33. Dong W, Li Y, Sheng X, Zhu X. Trajectory estimation of a flying robot with a single ranging beacon and derived velocity constraints. *IEEE Trans Ind Electron* 2023;70:5024–33. DOI
34. Yu X, Lu L. Distributed formation control of nonholonomic vehicles subject to velocity constraints. *IEEE Trans Ind Electron* 2016;63:1289–98. DOI
35. Khaledyan M, Liu T, Fernandez-Kim V, de Queiroz M. Flocking and target interception control for formations of nonholonomic kinematic agents. *IEEE Trans Contr Syst Technol* 2020;28:1603–10. DOI
36. Shevitz D, Paden B. Lyapunov stability theory of nonsmooth systems. *IEEE Trans Autom Control* 1994;39:1910–4. DOI
37. Slotine JJE, Li W. Applied nonlinear control. Prentice-Hall, Inc.; 1991. Available from: https://lewisgroup.uta.edu/ee5323/notes/Slotine%20and%20Li%20applied%20nonlinear%20control-%20bad%20quality.pdf. [Last accessed on 7 Nov 2024].